Supplementary Information

Theoretical design principles of Single-Atom Alloys Catalysts for CO Preferential Oxidation from High-Throughput First-Principles Microkinetics

Zhang Liu,[†,‡] Yanfei Liu,[†] Yanwei Wen,[†] Zhaojie Wang,[†] Limin Guo,[‡] Rong Chen,[§] Aimin Zhang,[*,¶] and Bin Shan[*,†]

[†] *School of Materials Science and Engineering, Huazhong University of Science and Technology, Wuhan 430074, P.R. China*

[‡] *School of Environmental Science and Technology, Huazhong University of Science and Technology, Wuhan 430074, P.R. China*

[§] *School of Mechanical Science and Engineering, Huazhong University of Science and Technology, Wuhan 430074, P.R. China*

[¶] *State Key Laboratory of Precious Metal Functional Materials, Kunming 650106, P.R. China*

* Corresponding authors

E-mail: aimin.zhang@ipm.com.cn; bshan@mail.hust.edu.cn

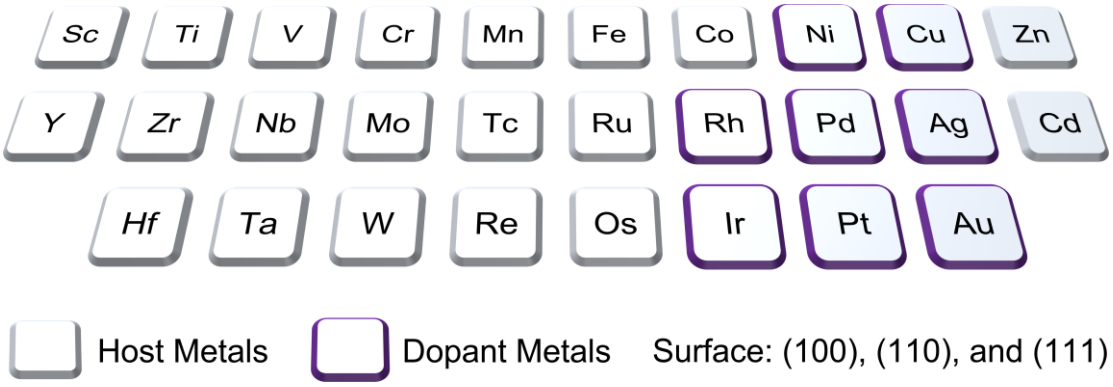

Fig. S1. The 672 candidate SAAs encompass single-atom dopants from 3*d*, 4*d*, and 5*d* transition metals, the host metals circled by purple lines, and three low-index surfaces.

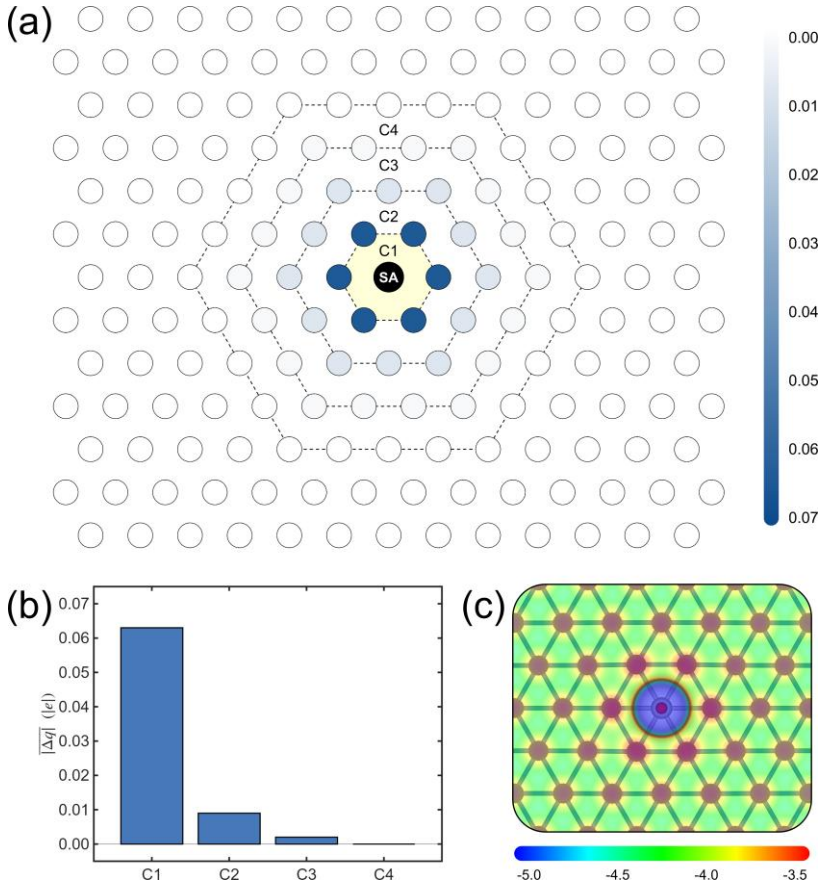

Fig. S2 (a) Bader charge changes of Pt_1@Cu(111) relative to bare Cu(111) p(9×9) surface and (b) the average value of each circle enclosed by the black wireframe form Pt_1 center to the inside out (C1, C2, C3, and C4). (c) Surface electrostatic potential map of Pt_1@Cu(111) with CO adsorbed on Pt_1 site with 5×10^{-3} e bohr^{-3} isosurface level. The (co)adsorbed species in contact with the shaded area in (a) are considered as a "state".

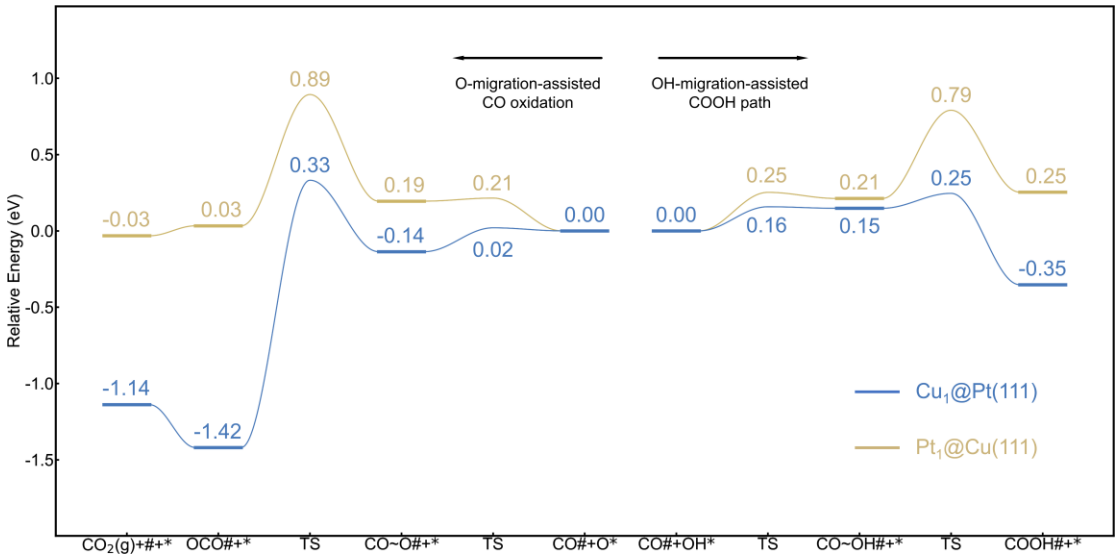

Fig. S3 Energy profiles of O/OH-migration-assisted CO oxidation and COOH path on Pt_1@Cu(111) and Cu_1@Pt(111) SAAs. Given that the transition state energies for species diffusion closely match those of the initial or final states, and the diffusion barriers are markedly lower than the combination barriers of $CO^{\#}$ and O*/OH*, we rationalize the process of species migration from host sites to SA sites and subsequent reaction via a single elementary step, for instance, $CO^{\#} + OH^* \rightarrow COOH^{\#} + *$.

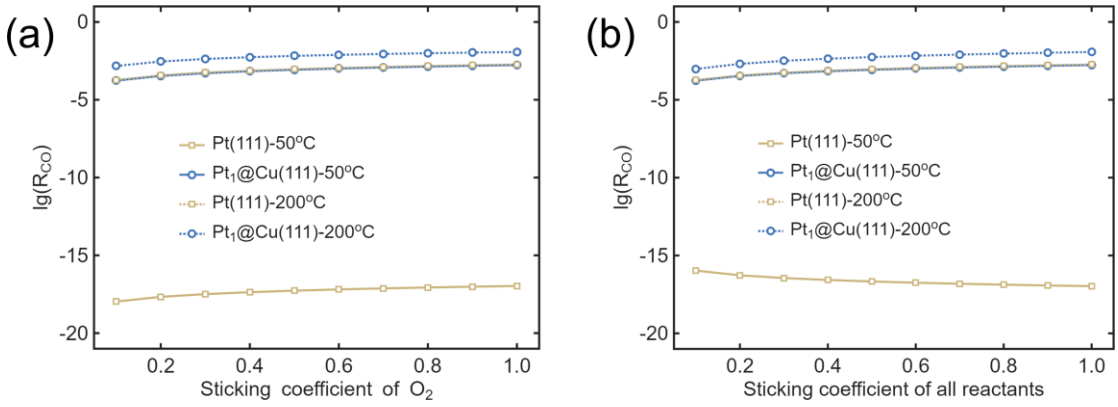

Fig. S4 Overall CO oxidation reaction rates on Pt(111) and Pt_1@Cu(111) at 50 and 200 ℃ varying the sticking coefficient of (a) O_2 and (b) all reactants between 0.1 and 1.

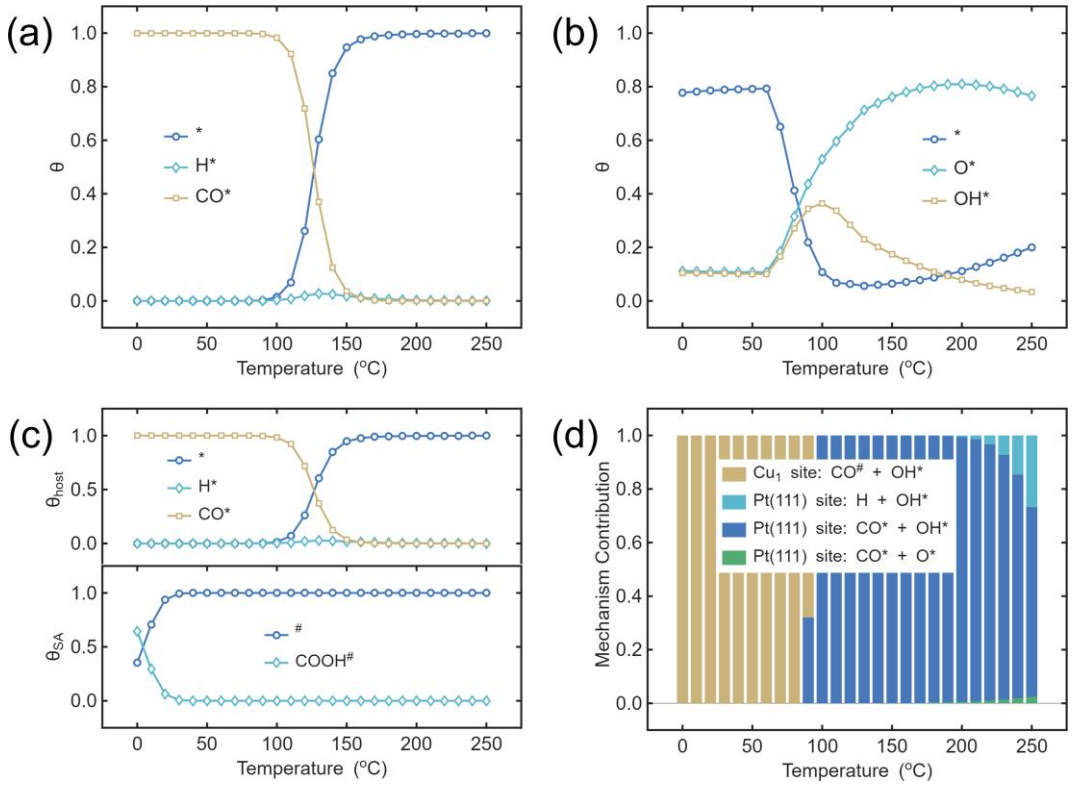

Fig. S5 Coverage profiles of (a) Pt(111), (b) Cu(111), and (c) Cu_1@Pt(111) for CO PROX full networks, respectively. (d) Mechanism contribution based on combined reaction rates of CO_2 and H_2O production on Cu_1@Pt(111).

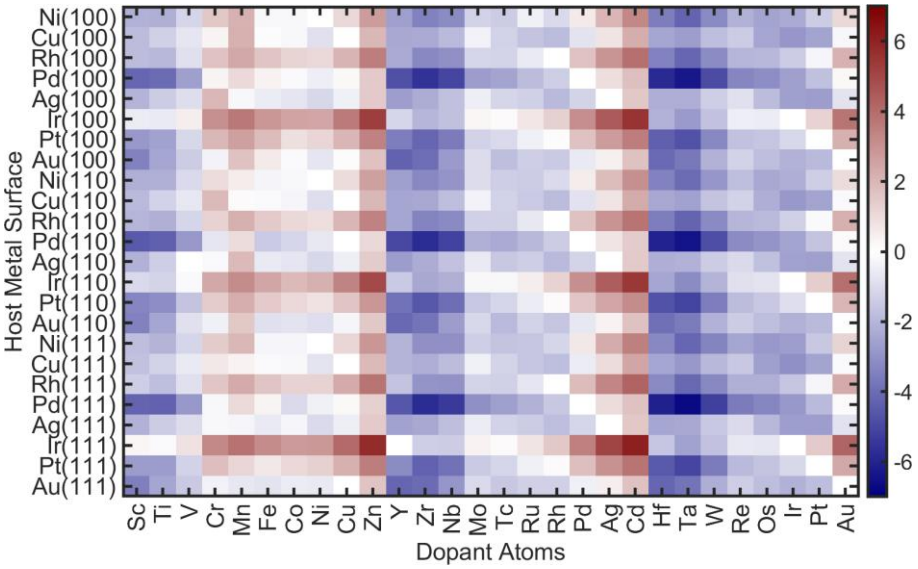

Fig. S6 Formation energies (Units: eV) of all SAAs.

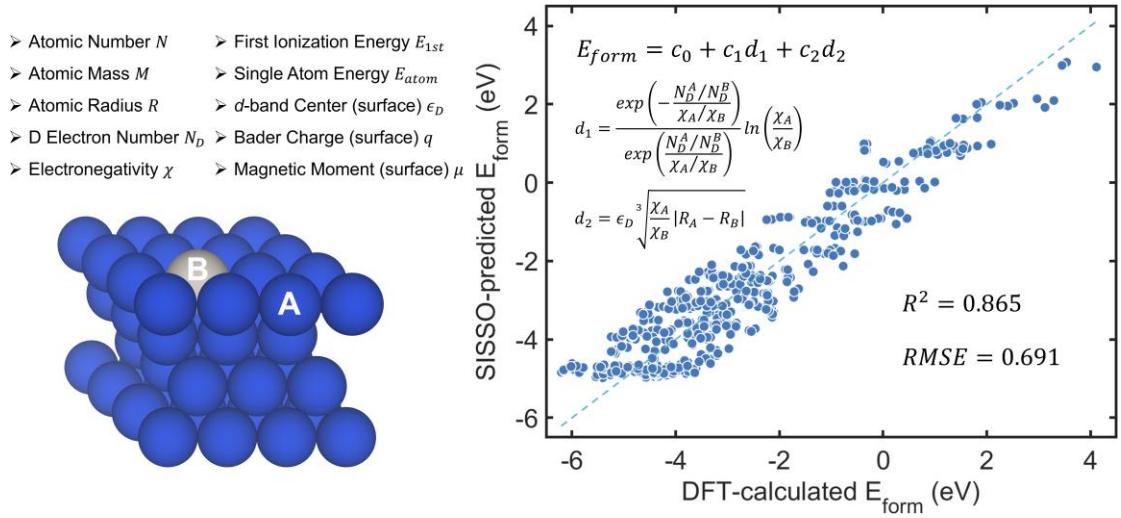

Fig. S7 SISSO regression training performed on structural descriptors relative to intrinsic properties of SAAs.

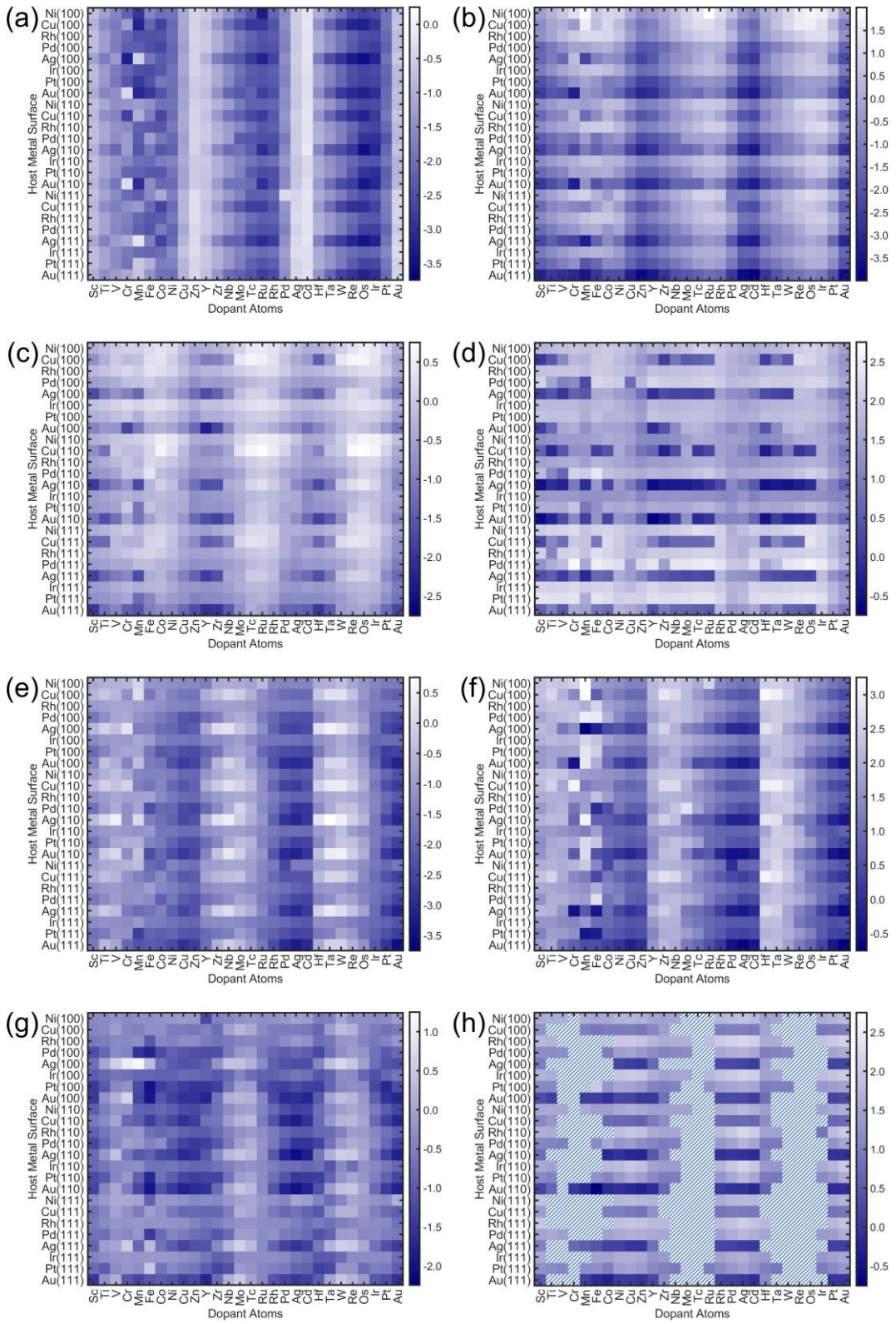

Fig. S8 Reaction heat (Units: eV) of (a) $CO(g) + {}^{\#} \rightarrow CO^{\#}$, (b) $CO^{\#} + O^{*} \rightarrow OCO^{\#} + {}^{*}$, (c) $CO^{\#} + OH^{*} \rightarrow COOH^{\#} + {}^{*}$, (d) $CO^{\#} + H^{*} \rightarrow HCO^{\#}$, (e) $OO^{\#} + CO(g) \rightarrow OCOO^{\#}$, (f) $OH^{\#} + H^{*} \rightarrow HOH^{\#}$, (g) $OO^{\#} + H_2(g) \rightarrow OH{\sim}OH^{\#}$, and (h) $OO^{\#} + H^{*}$

→ $OOH^{\#}$ + *. The shaded region in (h) represent that the $OOH^{\#}$ is thermodynamically unstable and hard to form.

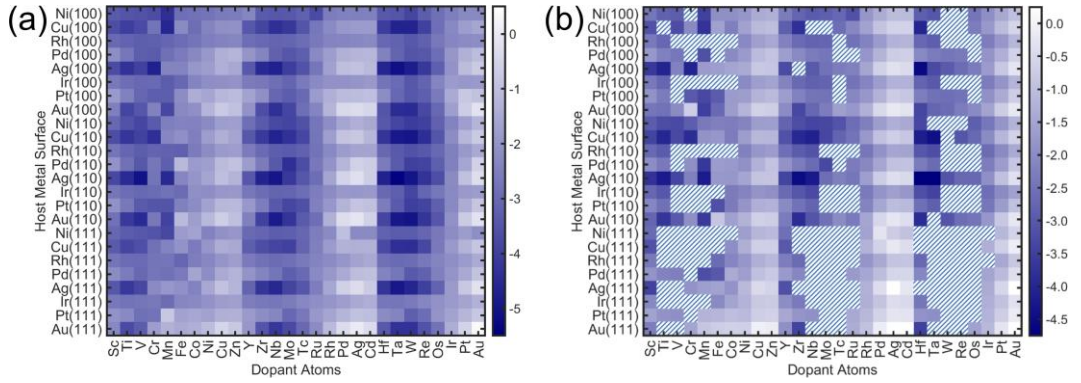

Fig. S9 Adsorption energies (Units: eV) of (a) $O^{\#}$ and (b) $OO^{\#}$ at SA sites. The shaded region in (b) represent the spontaneous decomposition of $OO^{\#}$ to $O{\sim}O^{\#}$.

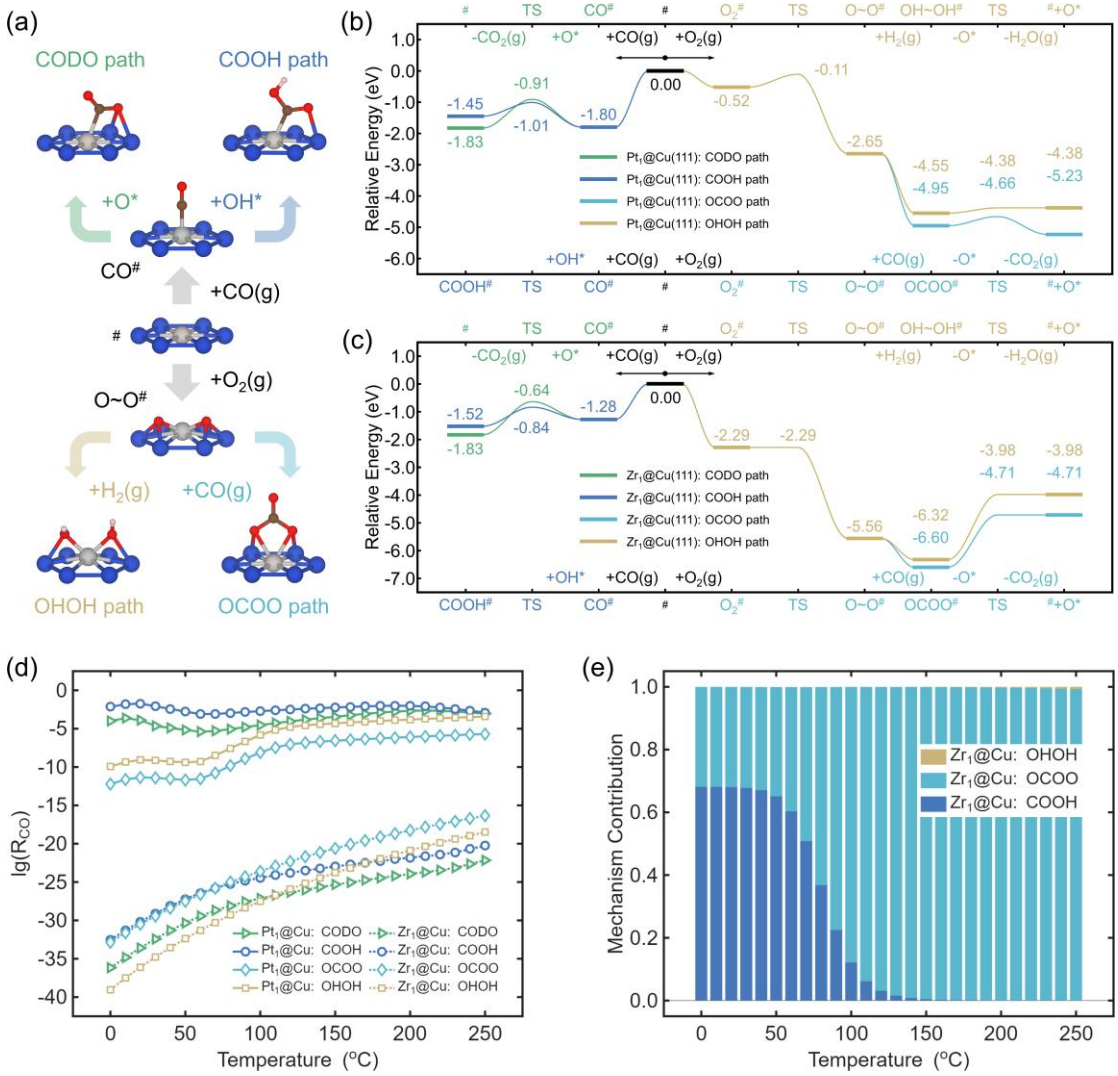

Fig. S10 (a) Schematic illustration of the simplified reaction network comprising two scenarios: CO-preferential adsorption and O_2-preferential adsorption at the single-atom site. Energy profiles of the key steps in the simplified network at (b) Pt_1@Cu(111) and (c) Zr_1@Cu(111). (d) Reaction rates of distinct pathways at the Pt_1 and Zr_1 sites and (e) mechanism contribution at the Zr_1 site.

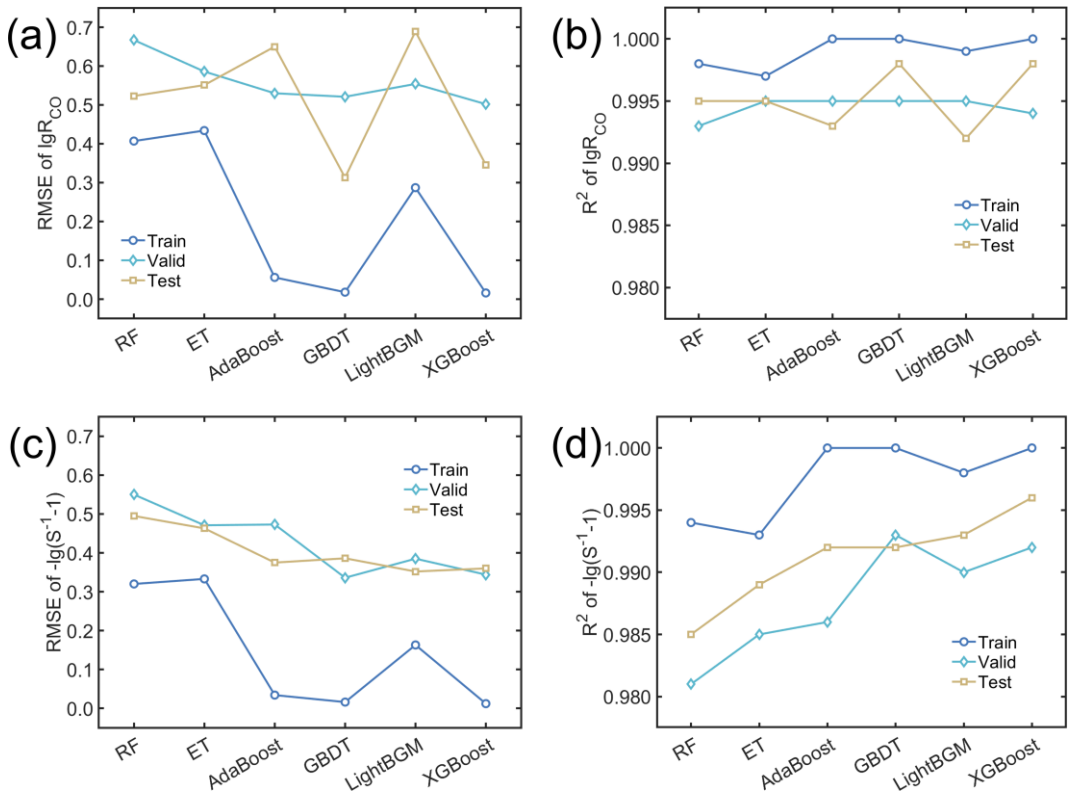

Fig. S11 Performance of different ML methods.

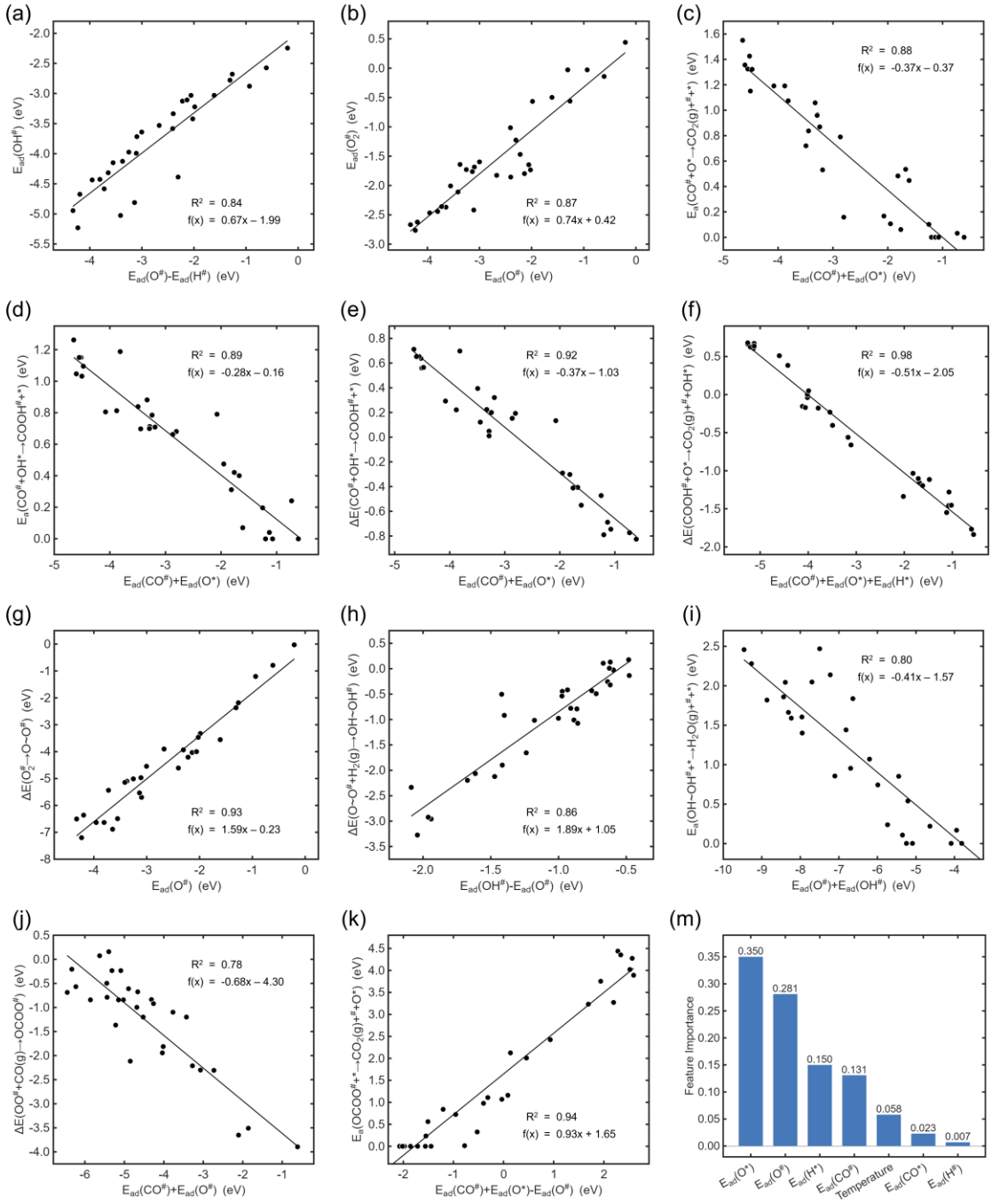

Fig. S12 Key scaling relationships illustrating the dependencies of the following energy parameters on adsorption energies, corresponding to the data presented in Table S3: (a) $E_{ad}(OH^{\#})$, (b) $E_{ad}(O_2^{\#})$, (c) $E_a(CO^{\#}+O^* \rightarrow CO_2(g)+^{\#}+*)$, (d) $E_a(CO^{\#}+OH^* \rightarrow COOH^{\#}+*)$, (e) $\Delta E(CO^{\#}+OH^* \rightarrow COOH^{\#}+*)$, (f) $\Delta E(COOH^{\#}+O^* \rightarrow CO_2(g)+^{\#}+OH^*)$, (g) $\Delta E(O_2^{\#} \rightarrow O{\sim}O^{\#})$, (h) $\Delta E(O{\sim}O^{\#}+H_2(g) \rightarrow OH{\sim}OH^{\#})$, (i) $E_a(OH{\sim}OH^{\#}+* \rightarrow H_2O(g)+O^*)$, (j) $\Delta E(O{\sim}O^{\#}+CO(g) \rightarrow OCOO^{\#})$ and (k) $E_a(OCOO^{\#}+* \rightarrow CO_2(g)+^{\#}+O^*)$. (m) Intrinsic feature importance scores of the GBDT model.

The linear correlations among the energetic parameters from Table S3 are presented in Fig. S12a-k. The correlations reveal that the energy parameters of the main pathways in the simplified network can be linearly expressed in terms of the adsorption energies of CO, O atom, and H atom at both the host and the SA sites. For instance, the adsorption energy of O_2 at the SA site ($E_{ad}(O_2^{\#})$) exhibits a strong linear correlation with $E_{ad}(O^{\#})$, indicating that $E_{ad}(O^{\#})$ effectively reflects the O_2 binding affinity of the SA site and therefore influences the competitive adsorption between CO and O_2 at the SA site. The intrinsic feature importance scores from the GBDT model are shown in Fig. S12m. The adsorption energy of O atoms at the host metal sites ($E_{ad}(O^*)$) exhibits the highest importance. In addition to its correlations with the ΔE and E_a of multiple steps, $E_{ad}(O^*)$ reflects the oxygen activation capability of the host sites. This ability of the host sites to provide active oxygen species (O*/OH*) is essential for the SAAs where CO preferentially adsorbs at the SA site, consistent with the observation in Section 3.1 that O_2 dissociation on Cu(111) serves as the RDS for Pt_1@Cu(111). When the analysis is restricted to the Cu(111)-based SAA subset, all the adsorption energies on the host metal are identical. And given the relatively low feature importance of $E_{ad}(H^{\#})$, $E_{ad}(CO^{\#})$ and $E_{ad}(O^{\#})$ are considered as the key descriptors governing the CO-PROX performance of Cu(111)-based SAAs.

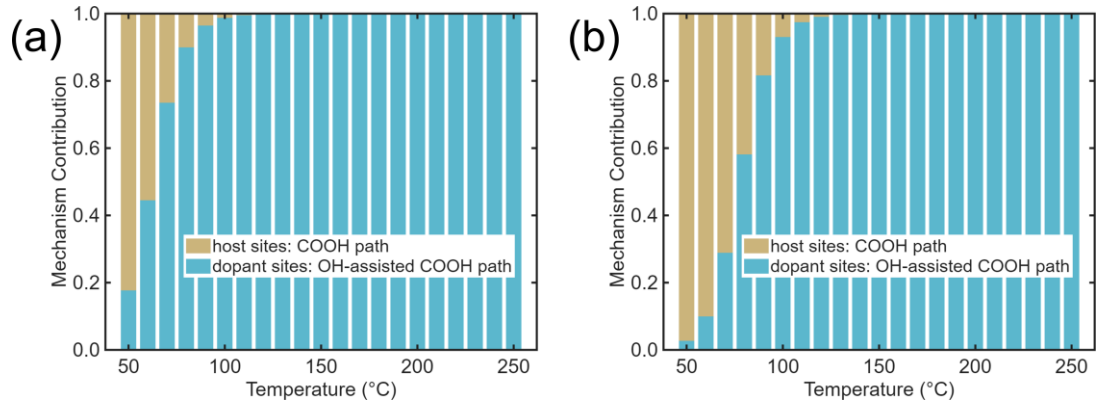

Fig. S13 Mechanism contribution of (a) Rh_1@Cu(111) and (b) Rh_1@Ag(111).

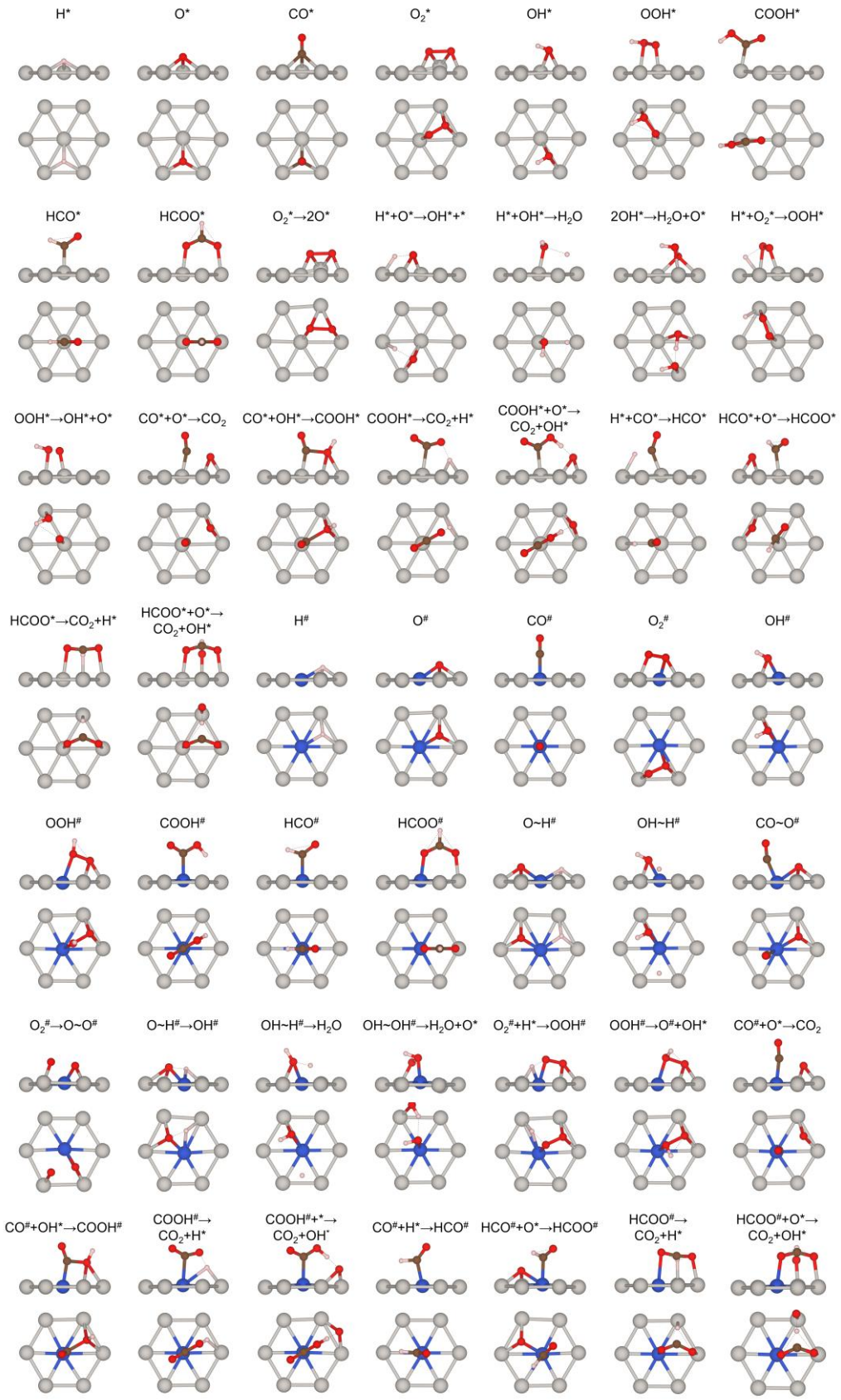

Fig. S14 Typical configurations of adsorption and transition state at Pt(111) and Cu_1 sites of Cu_1@Pt(111) related to Table S2.

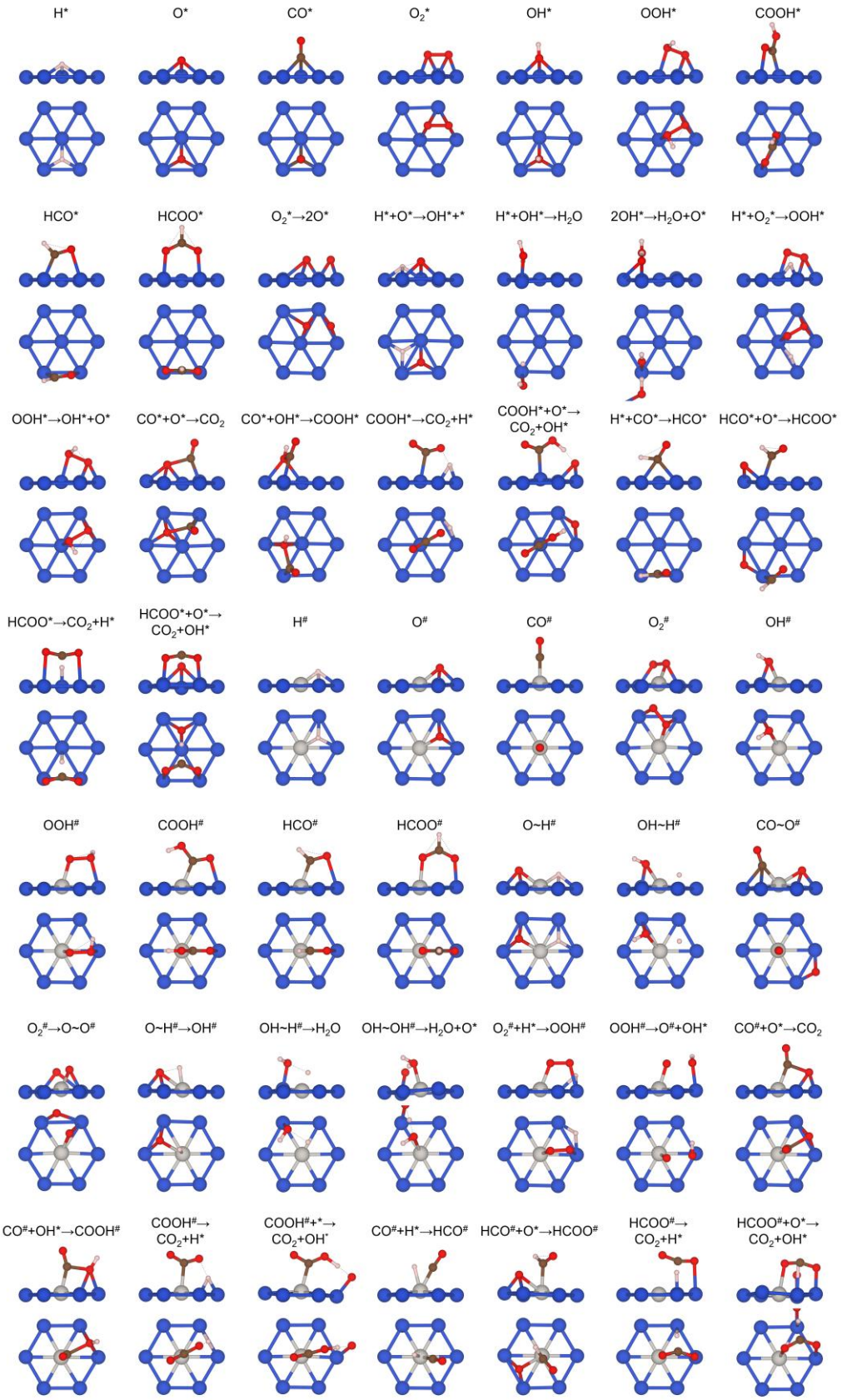

101

102 **Fig. S15** Typical configurations of adsorption and transition state at Cu(111) and Pt_1

103 sites of Pt_1@Cu(111) related to Table S2.

Steady-state condition

In the steady-state condition, the accumulation rates of each surface species *j* are in the form of Eq. S1, where $v_{j,i}$ is the stoichiometry of species *j* in the reaction step *i* (A negative value if *j* is a reactant and positive value if it is a product).

$$\frac{d\theta_j}{dt} = \sum_i v_{j,i} r_i = 0 \tag{S1}$$

For a dual-site model with 10% SA sites ($^{\#}$) and 90% host sites (*), combining with site conservation constraint in Eq. S2, a set of algebraic equations about the amount of surface species are established to accurately calculate surface species coverage (θ) and turnover frequency (TOF). The coverage data presented in related figures have been normalized with respect to the type of site.

$$\sum_j \theta_j = \sum_{m \in \text{SA sites}} \theta_m + \sum_{n \in \text{host sites}} \theta_n = 0.1 + 0.9 = 1.0 \tag{S2}$$

Enthalpy, Entropy and Gibbs Free Energy Calculation

The enthalpy is calculated by Eq. S3. E_{DFT}, E_{ZPE} and C are the calculated electronic energy, zero-point energy and heat capacity, respectively. The E_{ZPE} is calculated by Eq. S4 and ω_i are the vibrational frequencies of surfaces species by fixing the atoms that do not participate in the entire PROX process. As for heat capacity contribution, on the one hand, constant pressure heat capacities (C_P) for the gaseous reactant are adopted which are well-described by the polynomial as the function of temperature and the corresponding parameters of polynomial are obtained by regression of published heat capacity data. In our work, the third-order polynomial is utilized to determine the heat capacity. On the other hand, the heat capacity contribution of adsorbed states is calculated via Eq. S5. Note that the heat capacity contribution on enthalpy change is small. Eq. S6-S8 give the Gibbs free energy, enthalpy and entropy change and Eq. S9-

10 give the entropy of gas and adsorbed specie. The entropies of adsorbed species were calculated within the harmonic oscillator approximation. Extremely low-frequency modes (< 60 cm^{-1}) are reset to this threshold to prevent unphysically large entropy contributions[1,2]. It should be noted that a more complete treatment would include entropy contributions from hindered translations and rotations parallel to the surface, as well as a concentration-dependent term, as described in the advanced model developed by Sprowl et al.[3]. While our simplified approach may overestimate certain entropy contributions, we expect it to have a minimal impact on the comparative trends and mechanistic insights that are the focus of this study.

$$H = E_{DFT} + E_{ZPE} + \int_0^T C dT \tag{S3}$$

$$E_{ZPE} = 0.5 \sum h\omega_i \tag{S4}$$

$$\int_0^T C_{V,vib} dT = \sum_i^{\#vibs} \frac{h\omega_i}{e^{h\omega_i/k_B T} - 1} \tag{S5}$$

$$\Delta G_i = \Delta H_i - T\Delta S_i \tag{S6}$$

$$\Delta H_i = \sum_{j \in products} H_{j,i} - \sum_{j \in reactants} H_{j,i} \tag{S7}$$

$$\Delta S_i = \sum_{j \in products} S_{j,i} - \sum_{j \in reactants} S_{j,i} \tag{S8}$$

$$S_{gas} = A ln(t) + Bt + C\frac{t^2}{2} + D\frac{t^3}{3} - E\frac{t^{-2}}{2} + G \tag{S9}$$

$$S_{state} = k_B \sum_i^{\#vibs} \left[\frac{\varepsilon_i}{k_B T \left(e^{\frac{\varepsilon_i}{k_B T}} - 1 \right)} - ln\left(1 - e^{\frac{-\varepsilon_i}{k_B T}} \right) \right] \tag{S10}$$

137 **Table S1**. Parameter values in ML.

ML methods	Parameter Name	Parameter Values
RF	Node splitting evaluation criterion	mse
	Minimum sample size for internal node splitting	2
	Minimum sample size for leaf nodes	1
	Minimum sample weight for leaf nodes	0
	Maximum depth of the tree	10
	Maximum number of leaf nodes	50
	Threshold for node splitting impurity	0
	Number of decision trees	100
	Sampling with replacement	True
ETR	Node splitting evaluation criterion	mse
	Minimum sample size for internal node splitting	2
	Minimum sample size for leaf nodes	1
	Minimum sample weight for leaf nodes	0
	Maximum depth of the tree	10
	Maximum number of leaf nodes	50
	Threshold for node splitting impurity	0
	Number of decision trees	100
	Sampling with replacement	True
AdaBoost	Base learner	decision tree
	Number of base learners	100
	Loss function	linear
	Learning rate	1
GBDT	Loss function	friedman_mse
	Node splitting evaluation criterion	friedman_mse
	Number of base learners	100
	Learning rate	0.1
	Sampling proportion without replacement	1
	Minimum sample size for internal node splitting	2
	Minimum sample size for leaf nodes	1
	Minimum sample weight for leaf nodes	0
	Maximum depth of the tree	10

	Maximum number of leaf nodes	50
	Threshold for node splitting impurity	0
LightBGM	Base learner	gbdt
	Number of base learners	100
	Learning rate	0.1
	L1 regularization term	0
	L2 regularization term	1
	Feature sampling rate	1
	Tree feature sampling rate	1
	Node splitting threshold	0
	Minimum sample weight for leaf nodes	0
	Maximum depth of the tree	10
	Minimum sample size for leaf nodes	10
XGBoost	Base learner	gbtree
	Number of base learners	100
	Learning rate	0.1
	L1 regularization term	0
	L2 regularization term	1
	Feature sampling rate	1
	Tree feature sampling rate	1
	Node feature sampling rate	1
	Minimum sample weight for leaf nodes	0
	Maximum depth of the tree	10
SISSO	Dimension of the Descriptor	1/2/3
	Number of scalar features	17
	Maximal Feature Complexity	6
	Number of features in each SIS subspace	2000
	Metric for model selection in regression	RMSE
	Fit to a nonzero intercept for the linear model	True
	fmax_min	1e-3
	fmax_max	1e5

Table S2. The forward and reverse barriers (E_a^+ and E_a^-) and reaction energies (ΔE) of elementary steps (Unit: eV) and the corresponding forward and reversed rate constants (k^+ and k^-) at 300 K (Unit: s^{-1}). ΔE is calculated as $\Delta E = E_{products} - E_{reactants}$ (Negative values correspond to exothermic steps). The "/" in the E_a^+ and E_a^- columns indicate adsorption processes, with rate constants calculated via collision theory.

Elementary Steps	Pt_1@Cu(111)					Cu_1@Pt(111)				
	E_a^+	E_a^-	ΔE	k^+	k^-	E_a^+	E_a^-	ΔE	k^+	k^-
ES1: $H_2(g) + 2* = 2H*$	/	0.60	-0.60	3.23E+04	3.54E+02	/	1.09	-1.09	3.23E+04	6.25E-06
ES2: $O_2(g) + * = O_2*$	/	0.89	-0.89	8.07E+03	9.05E-04	/	0.69	-0.69	8.07E+03	1.87E-03
ES3: $O_2* + * = 2O*$	0.33	2.33	-2.00	1.70E+07	5.14E-27	0.43	2.17	-1.74	4.47E+05	3.08E+01
ES4: $H* + O* = OH* + *$	0.96	1.28	-0.32	5.01E-04	1.67E-09	0.96	1.27	-0.31	4.08E-04	2.47E-09
ES5: $H* + OH* = H_2O(g) + 2*$	0.96	/	0.18	5.29E-04	1.08E+04	1.03	/	-0.18	3.15E-05	1.08E+04
ES6: $2OH* = H_2O(g) + O* + *$	0.78	/	0.77	5.97E-07	1.08E+04	0.02	/	-0.14	7.74E+08	1.08E+04
ES7: $H* + O_2* = OOH* + *$	0.64	1.25	-0.61	7.17E+02	8.31E-07	0.87	1.02	-0.15	4.39E-01	1.81E-02
ES8: $OOH* + * = O* + OH*$	0.02	2.23	-2.21	8.98E+11	1.03E-24	0.08	1.71	-1.63	4.97E+10	5.57E-16
ES9: $H_2(g) + O* + * = H* + OH*$	/	1.49	-1.49	3.23E+04	1.02E-09	/	1.54	-1.54	3.23E+04	2.52E-11
ES10: $CO(g) + * = CO*$	/	0.93	-0.93	8.62E+03	1.16E+09	/	1.90	-1.90	8.62E+03	2.45E-07
ES11: $CO* + O* = CO_2(g) + 2*$	0.62	/	-0.79	2.49E+02	6.88E+03	0.86	/	-0.30	2.50E-02	6.88E+03
ES12: $CO* + OH* = COOH* + *$	0.61	0.61	-0.01	2.52E+02	3.54E+02	0.68	0.88	-0.20	2.30E+01	1.03E-02
ES13: $COOH* + * = CO_2(g) + H* + *$	0.32	/	-0.38	8.39E+10	6.88E+03	0.12	/	0.12	3.03E+15	6.88E+03
ES14: $COOH* + O* = CO_2(g) + OH* + *$	0.00	/	-1.05	4.48E+14	6.88E+03	0.48	/	0.25	3.09E+06	6.88E+03
ES15: $CO* + H* = HCO* + *$	1.02	0.10	0.92	1.46E-05	5.01E+10	1.25	0.29	0.96	9.93E-09	4.95E+08

ES16: HCO* + O* = HCOO* + *	0.11	2.14	-2.03	2.67E+10	1.58E-23	0.76	1.64	-0.88	5.10E-01	6.40E-15
ES17: HCOO* + * = CO_2(g) + H* + *	1.28	/	0.31	2.26E-06	6.88E+03	1.04	/	-0.11	9.84E-03	6.88E+03
ES18: HCOO* + O* = CO_2(g) + OH* + *	1.42	/	-0.36	9.82E-09	6.88E+03	2.20	/	-0.16	1.69E-22	6.88E+03
ES19: H_2(g) + $^{\#}$ + * = $H^{\#}$ + H*	/	0.74	-0.74	3.23E+04	1.74E+02	/	1.21	-1.21	3.23E+04	7.91E-07
ES20: O_2(g) + $^{\#}$ = $O_2^{\#}$	/	0.52	-0.52	8.07E+03	6.99E+04	/	0.59	-0.59	8.07E+03	3.83E+03
ES21: $O_2^{\#}$ + * = $O^{\#}$ + O*	0.09	2.13	-2.04	3.87E+10	1.44E-22	0.42	2.17	-1.75	1.42E+05	3.12E-23
ES22: $H^{\#}$ + O* = $OH^{\#}$ + *	1.12	1.24	-0.12	1.36E-05	4.06E-07	0.84	0.93	-0.09	7.29E-01	1.02E-01
ES23: $O^{\#}$ + H* = $OH^{\#}$ + *	0.77	1.24	-0.47	1.33E+01	4.06E-07	0.93	0.93	0.00	1.91E-02	1.02E-01
ES24: $OH^{\#}$ + H* = H_2O(g) + $^{\#}$ + *	0.53	/	-0.20	1.09E+05	1.08E+04	0.51	/	-0.08	1.05E+05	1.08E+04
ES25: $O_2^{\#}$ + H* = $OOH^{\#}$ + *	0.56	0.95	-0.39	8.86E+04	1.95E-01	0.44	0.46	-0.02	2.46E+05	1.06E+06
ES26: $OOH^{\#}$ + * = $O^{\#}$ + OH*	0.17	2.48	-2.31	4.25E+09	8.94E-29	0.00	1.62	-1.62	4.13E+11	1.31E-14
ES27: $OH^{\#}$ + OH* = H_2O(g) + $^{\#}$ + O*	0.41	/	0.41	1.51E+05	1.08E+04	0.38	/	-0.03	3.35E+07	1.08E+04
ES28: CO(g) + $^{\#}$ = $CO^{\#}$	/	1.80	-1.80	8.62E+03	4.13E-06	/	0.92	-0.92	8.62E+03	3.04E+09
ES29: $CO^{\#}$ + O* = CO_2(g) + $^{\#}$ + *	0.89	/	0.03	6.20E-02	6.88E+03	0.33	/	-1.14	5.20E+05	6.88E+03
ES30: $CO^{\#}$ + OH* = $COOH^{\#}$ + *	0.79	0.54	0.25	2.57E+01	3.82E+02	0.25	0.58	-0.33	8.84E+08	1.50E+00
ES31: $COOH^{\#}$ + * = CO_2(g) + $^{\#}$ + H*	0.12	/	0.12	4.11E+13	6.88E+03	0.36	/	-0.77	1.38E+09	6.88E+03
ES32: $COOH^{\#}$ + O* = CO_2(g) + $^{\#}$ + OH*	0.00	/	-0.41	2.51E+14	6.88E+03	0.39	/	-0.81	1.92E+07	6.88E+03
ES33: $CO^{\#}$ + H* = $HCO^{\#}$ + *	1.35	0.60	0.75	6.15E-10	4.42E+03	1.05	0.02	1.03	7.21E-07	4.86E+11
ES34: $HCO^{\#}$ + O* = $HCOO^{\#}$ + *	0.77	1.77	-1.00	2.38E-01	1.07E-17	0.00	2.00	-2.00	6.80E+11	3.92E-21
ES35: $HCOO^{\#}$ + * = CO_2(g) + $^{\#}$ + H*	1.31	/	0.22	3.64E-08	6.88E+03	0.86	/	-0.09	6.90E-01	6.88E+03

ES36: $HCOO^{\#} + O^{*} = CO_2(g) + {}^{\#} + OH^{*}$	1.52	/	-0.46	2.70E-10	6.88E+03	2.10	/	-0.14	2.38E-20	6.88E+03
ES37: $O_2{}^{\#} = O{\sim}O^{\#}$	0.41	2.13	-1.72	9.82E+05	9.01E-24	0.36	2.18	-1.82	4.98E+06	1.73E-24
ES38: $O{\sim}O^{\#} + H_2(g) = OH{\sim}OH^{\#}$	/	1.90	-1.90	3.23E+04	8.32E-13	/	1.75	-1.75	3.23E+04	3.29E-10
ES39: $OH{\sim}OH^{\#} + * = H_2O(g) + {}^{\#} + O^{*}$	0.17	/	0.16	8.35E+09	1.08E+04	0.40	/	0.08	1.37E+06	1.08E+04
ES40: $O{\sim}O^{\#} + CO(g) = OCOO^{\#}$	/	2.30	-2.30	8.62E+03	1.71E-14	/	2.23	-2.23	8.62E+03	2.86E-13
ES41: $OCOO^{\#} + * = CO_2(g) + {}^{\#} + O^{*}$	0.29	/	0.29	6.25E+07	6.88E+03	0.44	/	0.44	1.61E+05	6.88E+03

Shao et al. previously reported the adsorption strengths of CO and O on Pt(111) and Cu(111) surfaces[4]. In their work, the adsorption energies of CO on Pt(111) and Cu(111) were calculated to be -2.030 eV and -0.875 eV, respectively, while those of O atom were -1.194 eV and -1.626 eV. In the present study, the corresponding values are -1.901 eV and -0.930 eV for CO, and -1.215 eV and -1.454 eV for O atom. The two sets of results are in reasonable agreement, with deviations well within the typical range expected for DFT calculations using different setups.

Table S3. Energy parameters (Unit: eV) of 30 representative SAAs based on simplified CO PROX network.

Host metal	SA metal	E_1	E_2	E_3	E_4	E_5	E_6	E_7	E_8	E_9	E_{10}	E_{11}	E_{12}	E_{13}	E_{14}
Ni	Cr	-3.55	-2.08	-0.91	-4.15	-2.01	1.15	1.03	0.56	0.67	-6.50	-0.02	2.05	0.07	0.72
Ni	Rh	-2.22	-2.09	-0.58	-3.13	-1.47	1.43	1.15	0.64	0.61	-4.20	-0.78	0.11	-0.84	0.00
Ni	Re	-3.10	-2.22	-0.66	-3.72	-1.69	1.55	1.26	0.71	0.66	-5.70	0.13	1.44	-0.24	0.24
Cu	V	-3.65	-1.75	-0.50	-4.32	-2.37	0.53	0.71	0.32	-0.41	-6.88	0.11	1.60	0.16	2.01
Cu	Mn	-2.41	-1.36	-0.36	-3.59	-1.02	0.16	0.68	0.19	-0.66	-4.59	-1.01	0.74	-1.10	0.98
Cu	Ni	-1.98	-2.05	-0.62	-3.22	-0.56	0.72	0.84	0.39	-0.18	-3.33	-1.66	0.54	-1.94	0.56
Cu	Mo	-3.95	-2.38	-0.58	-4.44	-2.47	1.07	1.19	0.70	-0.16	-6.63	0.18	2.05	-0.21	2.13
Cu	Pd	-1.31	-1.43	-0.44	-2.78	-0.03	0.79	0.66	0.15	-0.56	-2.37	-2.12	0.00	-2.31	0.00
Cu	Pt	-1.27	-1.80	-0.48	-2.68	-0.56	0.87	0.78	0.20	-0.23	-2.18	-1.90	0.17	-2.30	0.00
Rh	Fe	-3.11	-2.34	-0.67	-4.00	-2.42	1.33	1.15	0.65	0.63	-4.97	-1.01	0.86	-0.50	0.00
Rh	Ru	-2.40	-2.26	-0.64	-3.33	-1.85	1.32	1.09	0.57	0.64	-4.61	-0.42	0.24	-0.67	0.00
Rh	Ir	-2.14	-2.39	-0.60	-3.11	-1.80	1.36	1.05	0.65	0.68	-4.03	-0.45	0.00	-1.20	0.00
Pd	Co	-1.61	-1.82	-0.62	-3.03	-0.50	1.06	0.88	0.22	-0.17	-3.56	-0.51	0.22	-1.20	0.00
Pd	Mo	-3.25	-1.77	-0.59	-3.97	-1.73	0.97	0.71	0.05	-0.04	-5.01	-0.49	2.14	-0.84	1.07
Pd	W	-3.37	-1.78	-0.54	-4.13	-1.64	0.96	0.70	0.01	0.00	-5.10	-0.43	2.47	-0.84	1.16
Ag	V	-3.80	-1.28	0.23	-4.43	-2.44	0.45	0.07	-0.55	-1.11	-6.64	0.01	1.59	-0.23	3.27
Ag	Cu	-0.94	-0.93	-0.02	-2.88	-0.03	0.10	0.20	-0.47	-1.55	-1.20	-2.96	0.00	-3.51	1.11

Ag	Y	-3.14	-0.88	-0.18	-4.81	-1.76	0.00	0.00	-0.79	-1.28	-5.54	-2.20	1.40	-1.81	3.75
Ag	Zr	-4.23	-1.63	-0.39	-5.23	-2.77	0.11	0.47	-0.29	-1.03	-7.20	-0.97	2.46	-0.84	4.44
Ag	Pd	-0.61	-1.49	-0.29	-2.57	-0.14	0.48	0.31	-0.30	-1.16	-0.79	-2.92	0.00	-3.65	0.84
Ag	Au	-0.21	-0.41	0.13	-2.25	0.44	0.03	0.24	-0.77	-1.77	-0.03	-3.27	0.00	-3.90	0.33
Ir	Os	-2.06	-2.21	-0.53	-3.03	-1.64	1.19	0.81	0.29	0.51	-4.00	-0.54	0.00	-0.92	0.00
Pt	Tc	-2.67	-2.23	-0.54	-3.53	-1.83	0.84	0.70	0.12	0.05	-3.90	-0.79	1.07	-0.61	0.01
Pt	Os	-2.02	-2.66	-0.51	-3.42	-1.73	1.19	0.81	0.22	0.38	-3.46	-0.92	0.85	-1.00	0.00
Au	Sc	-2.30	-0.97	0.00	-4.39	-1.23	0.00	0.00	-0.83	-1.84	-3.93	-2.33	0.95	-2.21	3.23
Au	Ti	-3.73	-1.49	-0.06	-4.58	-2.36	0.00	0.04	-0.69	-1.45	-5.43	-1.07	1.66	-1.37	3.89
Au	Nb	-4.19	-2.04	-0.17	-4.67	-2.62	0.54	0.40	-0.41	-1.20	-6.36	-0.13	1.82	-0.57	4.02
Au	Tc	-3.00	-2.43	-0.29	-3.64	-1.60	0.17	0.79	0.13	-1.34	-4.54	-0.25	1.84	-0.79	2.42
Au	Hf	-3.41	-1.44	-0.03	-5.02	-2.11	0.00	0.00	-0.75	-1.45	-5.14	-2.07	1.86	-2.12	4.35
Au	Ta	-4.33	-2.12	-0.16	-4.95	-2.67	0.06	0.42	-0.41	-1.10	-6.50	-0.32	2.28	-0.69	4.28

Notation: E_1: $E_{ad}(O^{\#})$; E_2: $E_{ad}(CO^{\#})$; E_3: $E_{ad}(H^{\#})$; E_4: $E_{ad}(OH^{\#})$: E_5: $E_{ad}(O_2{}^{\#})$; E_6: $E_a(CO^{\#}+O^* \rightarrow CO_2(g)+{}^{\#}+*)$; E_7: $E_a(CO^{\#}+OH^* \rightarrow COOH^{\#}+*)$; E_8: $\Delta E(CO^{\#}+OH^* \rightarrow COOH^{\#}+*)$; E_9: $\Delta E(COOH^{\#}+O^* \rightarrow CO_2(g)+{}^{\#}+OH^*)$; E_{10}: $\Delta E(O_2{}^{\#} \rightarrow O{\sim}O^{\#})$; E_{11}: $\Delta E(O{\sim}O^{\#}+H_2(g) \rightarrow OH{\sim}OH^{\#})$; E_{12}: $E_a(OH{\sim}OH^{\#}+* \rightarrow H_2O(g)+O^*)$; E_{13}: $\Delta E(O{\sim}O^{\#}+CO(g) \rightarrow OCOO^{\#})$; E_{14}: $E_a(OCOO^{\#}+* \rightarrow CO_2(g)+{}^{\#}+O^*)$.

Reference

1. H. Xiao, T. Cheng and W. Goddard. Journal of the American Chemical Society, 2017, 139, 130-136.
2. H. Xiao, T. Cheng, W. Goddard and R. Sundararaman. Journal of the American Chemical Society, 2016, 138, 483-486.
3. L. Sprowl, C. Campbell and L. Á rnadóttir. Journal of Physical Chemistry C, 2016, 120, 9719-9731
4. J. Zhang, Z. Wen, W. Wang, Y. Sun, D. Zhou, D. Wang, Q. Wang, X. Tan, X. Wu, X. Shao. Journal of Catalysis, 2023, 425, 1-7.